PAPER

Development of novel melt-processable biopolymer nanocomposites based on poly(L-lactic acid) and WS$_2$ inorganic nanotubes

Mohammed Naffakh,[*a] Carlos Marco[b] and Gary Ellis[b]

The use of tungsten disulphide inorganic nanotubes (INT-WS$_2$) offers the opportunity to produce novel and advanced biopolymer-based nanocomposite materials with excellent nanoparticle dispersion without the need for modifiers or surfactants *via* conventional melt blending. The study of the non-isothermal melt-crystallization kinetics provides a clear picture of the transformation of poly(L-lactic acid) (PLLA) molecules from the non-ordered to the ordered state. The overall crystallization rate, final crystallinity and subsequent melting behaviour of PLLA were controlled by both the incorporation of INT-WS$_2$ and the variation of the cooling rate. In particular, it was shown that INT-WS$_2$ exhibits much more prominent nucleation activity on the crystallization of PLLA than other specific nucleating agents or nano-sized fillers. These features may be advantageous for the enhancement of mechanical properties and process-ability of PLLA-based materials. PLLA/INT-WS$_2$ nanocomposites can be employed as low cost biodegradable materials for many eco-friendly and medical applications, and the exceptional crystallization behaviour observed opens new perspectives for scale-up and broader applications.

1. Introduction

Poly(lactic acid) (PLA) has been intensively investigated because it is biodegradable, can be produced from renewable resources like corn and sugar cane, is nontoxic to the human body and the environment and can be composted.[1,2] Since its degradation products are bioresorbable, this polymer is one of those selected as appropriate for use in biomedical and pharmaceutical applications such as surgical sutures, bone fixation devices, and controlled drug release matrices.[3] Over the past decade, the discovery of new polymerization routes that allow the economical production of high molecular weight PLA, along with the elevated environmental awareness of the general public, has resulted in an expanded use of PLA for consumer goods and packaging applications.[4–6] Furthermore, with regard to its favorable biodegradability, renewability, reasonably good mechanical properties and versatile fabrication methods, PLA is well positioned as a key material for the substitution of petroleum-based polymers.[5] Poly(L-lactic acid) (PLLA) is a typical stereoisomer of PLA and this semicrystalline polymer has good mechanical properties that are comparable to polyethylene, polypropylene and polystyrene. However, PLLA also exhibits some disadvantages. It exhibits a glass transition temperature (T_g) of about 60 °C, and therefore excellent mechanical properties cannot be preserved at relatively higher temperatures ($>T_g$). Furthermore, although PLLA is semicrystalline, it has poor crystallizability and is usually found in the amorphous state due to poor chain segment mobility that prevents the formation of stable nuclei and the growth of lamellae. Thus, the improvement in the thermal properties and crystallizability of PLLA has been the subject of an important research effort.[7]

The addition of fillers is one of the most cost-effective methods to improve the physical properties of polymeric materials. Fillers or additives for PLLA include nucleating agents and low-cost engineering polymers. The former increases the crystallinity of the material in a short period of thermal treatment and the latter reduces the overall cost of the polymeric materials. Effective nucleating agents reported for PLLA are talc,[8] uracil,[9] N,N'-bis(benzoyl) suberic acid dihydrazide,[10] and phenylphosphonic acid,[11] whilst nano-clay (MMT),[12] carbon nanotubes (CNTs),[13,14] nano-calcium carbonate (CaCO$_3$),[11] nano-zinc citrate (ZnCC),[15] graphene oxide (GO)[16] and (C60) fullerenes[13] are known as nanocomposite-forming additives. However, the fabrication of high quality nanocomposites normally requires chemical treatment to reduce the surface energy in order to ensure good particle

[a] *Universidad Politécnica de Madrid, Departamento de Ingeniería y Ciencia de los Materiales, Escuela Técnica Superior de Ingenieros Industriales, José Gutiérrez Abascal 2, 28006 Madrid, Spain. E-mail: mohammed.naffakh@upm.es*
[b] *Instituto de Ciencia y Tecnología de Polímeros (ICTP-CSIC), Juan de la Cierva 3, 28006 Madrid, Spain*

dispersion and strong interaction and adhesion between the nanofiller and polymer matrix. These requirements still pose great difficulties for nanoparticle filled polymer composites.

For these reasons the use of alternative filler particle types, such as inorganic fullerenes (IFs) and nanotubes (INTs) based on layered metal dichalcogenides such as WS_2 and MoS_2, becomes increasingly important. The first synthesis of such nanoparticles was reported by Tenne et al. in 1992 and 1993.[17,18] Since then the synthetic technology has advanced considerably and almost pure materials (>99%) are now available at industrial scales.[19,20] The synthetic process is catalyst-free, and the precursors (e.g. tungsten oxide and H_2S or sulfur) are relatively inexpensive. The moderate cost of such nano-structures has opened potential applications in catalysis, rechargeable batteries, drug delivery, solar cells and electronics and, more recently, in the field of polymer nanocomposites.[21] In this respect, WS_2 nanotubes (INT-WS_2) have been used as reinforcing agents to improve the mechanical and tribological properties of epoxy composites,[22] electrospun poly(methyl methacrylate) fibers[23] and poly(propylene fumarate) (PPF) nanocomposites.[24]

To the best of our knowledge, this is the first report on the preparation and characterization of biodegradable PLLA polymer nanocomposites based on environmentally friendly inorganic nanotubes (INT-WS_2). In this study, we have analyzed the effects of INT-WS_2 loading on the structure–property–performance relationship of a series of PLLA/INT-WS_2 nanocomposites. In particular, the crystallization and melting behaviour of PLLA/INT-WS_2 were investigated by differential scanning calorimetry (DSC) and time-resolved synchrotron X-ray diffraction under dynamic conditions, similar to the industrial processing conditions for polymers. These observations will enable the development of novel melt-processable PLLA/INT-WS_2 nanocomposites with improved thermal and mechanical properties for many eco-friendly (e.g. packaging) applications, biomedical applications (e.g. surgical sutures, bone fixation devices, etc.) and general-purpose plastic fields.[1,5,6]

2. Experimental section

2.1. Materials and processing

The biopolymer matrix was poly(L-lactic acid) (PLLA) purchased from Goodfellow Ltd. (density = 1.25 g cm^{-3}, $M_w \approx 1.5 \times 10^5$ g mol^{-1}). Multiwall WS_2 1D nanotubes (INT-WS_2) with diameters of 30–150 nm and lengths of 1–20 μm were obtained from NanoMaterials Ltd. (Israel). Transmission electron microscopy (TEM) analysis of one such nanotube has shown that the typical INTs are 50–100 nm thick made of 20–30 layers with an interlayer spacing of about 0.62 nm.[22,23] Each mixture of PLLA and INT-WS_2 (0.1, 0.5 and 1.0 wt.%) was dispersed in a small volume of ethanol and homogenized by mechanical stirring and bath ultrasonication for approximately 10 min. Subsequently, the dispersion was partially dried under vacuum at 60 °C under a pressure of about 70 mbar for 24 h. The melt-mixing of the resulting dispersion was performed using a micro-extruder (Thermo-Haake Minilab system) operated at 190 °C and a rotor speed of 100 rpm for 10 min.

2.2. Characterization techniques

2.2.1. Scanning electron microscopy (SEM).
The dispersion of INT-WS_2 in the PLLA matrix was characterized using an ultra-high field-emission scanning microscopy (FESEM) (SU8000, Hitachi Co., Japan). Cryogenically fractured surfaces from film specimens were coated with a ~5 nm Au/Pd layer to avoid charging during electron irradiation.

2.2.2. Thermogravimetric analysis (TGA).
The thermal stability of the nanocomposites was analyzed in a TA Instruments Q50 thermobalance using a heating rate of 10 °C min^{-1} from 100 to 800 °C under an inert (nitrogen) atmosphere.

2.2.3. Differential scanning calorimetry (DSC).
The crystallization and melting behaviour of the nanocomposites were investigated using a Perkin Elmer DSC7/Pyris differential scanning calorimeter (Perkin-Elmer España SL, Madrid, Spain), calibrated with indium (T_m = 156.6 °C, ΔH_m = 28.45 kJ kg^{-1}) and zinc (T_m = 419.47 °C, ΔH_m = 108.37 kJ kg^{-1}). Samples of approximately 10 mg were studied in aluminium capsules under an inert nitrogen atmosphere with a flow rate of 25 ml min^{-1}. Prior to cooling, the samples were held at 225 °C for 5 min to erase any thermo-mechanical memory effects.

Under dynamic conditions, cooling cycles from the melt were undertaken for each sample at cooling rates (ϕ) of 1, 2, 5, 10 and 20 °C min^{-1}, followed by a heating cycle from 40 to 225 °C at 10 °C min^{-1}. The melting temperature (T_m) and the crystallization temperature (T_p) were determined from the maximum melting endotherm observed during the heating scan and the minimum crystallization exotherm observed during the cooling scan, respectively. The crystallinity was calculated as follows:

$$(1-\lambda) = \frac{\Delta H_c}{\Delta H_m^{0}} \tag{1}$$

where ΔH_c is the crystallization enthalpy and ΔH_m^{0} is the enthalpy of melting for perfect crystals: 93 J g^{-1}.[4,7,25]

2.2.4. Time-resolved synchrotron X-ray diffraction.
Wide-angle X-ray scattering (WAXS) experiments using synchrotron radiation were performed at the A2 beamline of the HASYLAB synchrotron facility (DESY, Hamburg). The experiments were performed with monochromatic X-rays of 0.15 nm wavelength using a germanium single crystal as the dispersing element. The scattering was detected with a linear Gabriel detector. Measurements were performed with an acquisition time of 60 s (wait time = 2 s and read time = 10 s) and 30 s (wait time = 20 s and read time = 10 s) for cooling and subsequent heating, respectively.

2.2.5. Dynamic mechanical analysis (DMA).
Dynamic mechanical analysis of the PLLA/INT-WS_2 nanocomposites was performed in tensile mode using a Mettler DMA861 on rectangular shaped bars with dimensions of 20 × 4 × 0.5 mm^3 in the temperature range between −100 and 150 °C at a heating rate of 3 °C min^{-1} and frequencies of 0.1, 1 and 10 Hz. A

dynamic force of 8 N oscillating at a fixed frequency and an amplitude of 17 μm were used.

3. Results and discussion

3.1. Dispersion of INTs in the PLLA matrix

It is well known that the state of dispersion of nanoparticles in a polymer matrix influences the physical properties of the polymer. To improve the mechanical and thermal performance of the polymer matrix, a fine dispersion of nanoparticles in the polymer matrix is usually required. SEM was used to observe the surfaces of PLLA/INT-WS$_2$ nanocomposites fractured in liquid nitrogen to observe the dispersion of INT-WS$_2$ in the PLLA matrix. Fig. 1a and b show an overview of the fracture surface of the PLLA/INT-WS$_2$ nanocomposites at 0.5 and 1.0 wt.%, respectively. It can be clearly seen that the processing of the PLLA/INT-WS$_2$ nanocomposites was effective with the INTs uniformly dispersed at the nanoscale in the PLLA matrix by the shear force encountered during melt-blending. A homogeneous dispersion of INT-WS$_2$ was also found for the PLLA/INT-WS$_2$ (99.9/0.1) sample. In no case was severe aggregation of non-modified INT-WS$_2$ observed in the PLLA matrix despite the INT loadings, indicating that the variation of INT-WS$_2$ contents from 0.1 to 1.0 wt.% does not significantly affect the dispersion and distribution of INT-WS$_2$ in the polymer matrix (Fig. 1b).
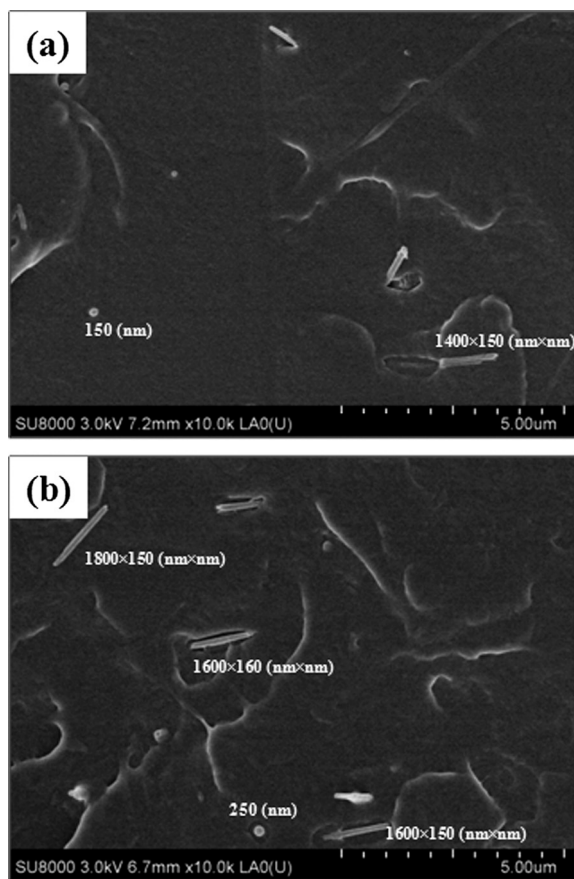

Fig. 1 High-resolution SEM image of PLLA nanocomposites: (a) PLLA/INT-WS$_2$ (0.5 wt.%) and (b) PLLA/INT-WS$_2$ (1.0 wt.%).

3.2. Thermal stability

As nanofillers generally affect the thermal stability of nano-composites, thermogravimetric analysis (TGA) of the PLLA/INT-WS$_2$ nanocomposites was carried out to establish the limiting processing conditions. In this respect, the addition of INTs may result in an improvement in the heat resistance of the polymer matrix due to their inherent high thermal stability.[23] However, analysis of the thermograms revealed that the INT-WS$_2$ had no influence on the characteristic degradation temperatures of PLLA, such as the temperature for 10% weight loss (T_{10}) and that corresponding to the maximum rate of weight loss (T_{mr}) that appeared at around 350 °C and 378 °C, respectively.

3.3. Non-isothermal melt-crystallization of neat PLLA and PLLA/INT nanocomposites at different INT loadings

It is well known that the crystalline morphology and structure obtained during the thermoplastic processing plays an important role in the physico-mechanical behaviour of the resulting PLLA, conditioning its potential uses.[26] In this way, the control of crystallization can be seen as a successful approach for improving the physico-mechanical properties of biopolymers. Semicrystalline polymers such as PLLA can crystallize from both molten and glassy states, which usually are termed as melt-crystallization and cold crystallization, respectively. As expected for thermoplastic materials, crystallized PLLA should exhibit higher stiffness and mechanical performance than the non-crystallized polymer. Thus, the suppression of molecular mobility by crystallization reduces the abrupt decrease in modulus at the glass transition temperature. Therefore, a detailed knowledge of the crystallization kinetics (rate of crystallization, size of crystallites, nucleation activity, effective energy barrier, *etc.*) and crystalline structure as well as the melting behaviour and how these affect several polymer properties is a key issue if polylactide derived products are to be tailored for different applications.

As described in the Experimental section, non-isothermal melt-crystallization of neat PLLA and its nanocomposites at different INT loadings was studied with DSC at various cooling rates ranging from 1 to 20 °C min^{-1}, corresponding to temperature changes that are found habitually in industrial applications. Fig. 2 shows the DSC cooling curves from pure PLLA and PLLA/INT-WS$_2$ nanocomposites obtained at different cooling rates. As shown in Fig. 2, the crystallization peak temperature (T_p) of PLLA was almost undetected at a high cooling rate, demonstrating that the crystallization of neat PLLA was very slow. On addition of INT-WS$_2$, a crystallization peak appeared in the DSC cooling curve. Compared to neat PLLA, the addition of inorganic nanotubes produced a shift in T_p to a higher temperature. On the other hand, the crystallization peak of PLLA containing INT-WS$_2$ sharpened in the cooling process, showing that INT-WS$_2$ acted as a nucleating agent for the crystallization and increased the overall crystallization rate of PLLA. For more clarity, Fig. 3 summarizes the variation of T_p with cooling rate and
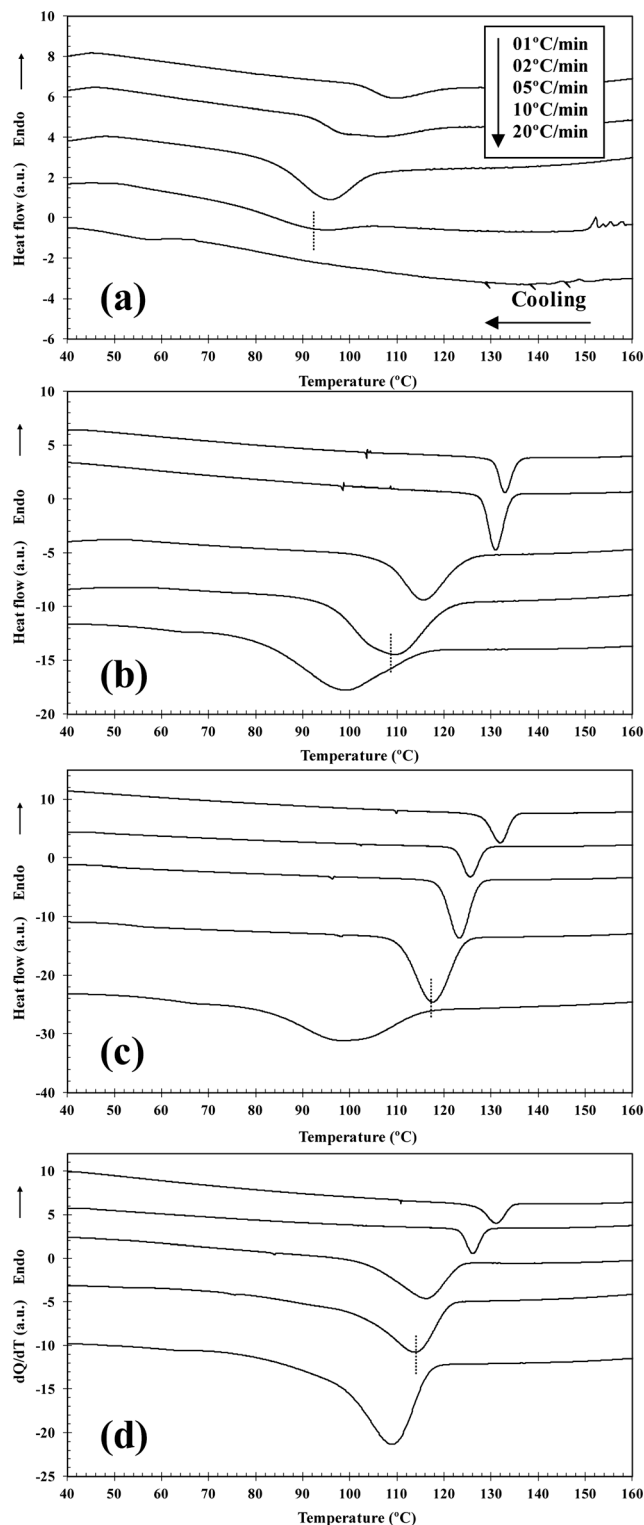
Fig. 2 DSC thermograms of the dynamic crystallization of (a) pure PLLA, (b) PLLA/INT-WS$_2$ (0.1 wt.%), (c) PLLA/INT-WS$_2$ (0.5 wt.%) and (d) PLLA/INT-WS$_2$ (1.0 wt.%) at the cooling rates indicated.

Fig. 3 Variation of the crystallization peak temperature (t_p) for PLLA/INT-WS$_2$ nanocomposites with (a) cooling rate and (b) composition.

composition, and two clear trends were observed. Firstly, an increase in the cooling rate resulted in a downward shift of T_p to the low-temperature range (Fig. 3a). Secondly, the INT-WS$_2$ showed an important capacity for accelerating the
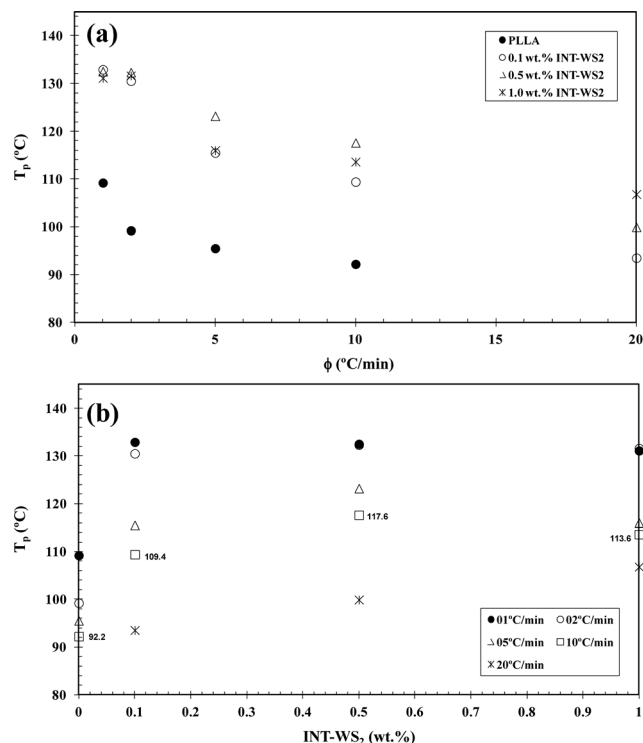
crystallization process (discussed later) due to a remarkable heterogeneous nucleation role in the nanocomposites. This effect was clearly observed to be a function of the composition (Fig. 3b) manifesting significant increases of around 17 °C in T_p, for example, with only 0.1 wt.% INT-WS$_2$ at a cooling rate of 10 °C min^{-1}. At a concentration of 0.5 wt.% of INT-WS$_2$ the value of T_p for PLLA continued to rise (*e.g.* 25 °C at 10 °C min^{-1}) and tended to stabilize for the highest concentration of 1.0 wt.%.

As discussed above, the overall nucleation and crystallization rates of PLLA under homogeneous conditions are relatively low. This has prompted tremendous efforts in the scientific community to improve the crystallization kinetics by adding nucleating agents to increase nucleation density and plasticizers to increase chain mobility. At high cooling rates (*e.g.* Fig. 2a) such as those encountered under conventional moulding conditions no crystallization is observed, and molded articles of poly(lactic acid) are typically obtained. As a result, the heat resistance such as heat distortion or heat deflection temperature (HDT) of the articles is very low, around 50–60 °C, due to the glass transition temperature (T_g) of poly(lactic acid).[27] Applications of PLLA as a neat resin are limited to disposable goods that do not require heat resistance. Thus, the lower HDT is an important bottleneck for the expansion and diversification of poly(lactic acid) applications.[5]

A series of effective nucleating agents have been reported for PLLA including talc,[8] uracil,[9] N,N′-bis(benzoyl) suberic acid dihydrazide,[10] and phenylphosphonic acid,[11] whilst nanoclay (MMT),[12] carbon nanotubes,[13,14] nano-calcium carbonate

Paper

Table 1 Melt-crystallization DSC data obtained at a cooling rate of 10 °C min^{-1} for different PLLA systems: T_p is the crystallization peak temperature and ΔT_p is the difference between the crystallization temperature peak of the composite and that of the neat matrix. n.p.: no peak was observed

Filler	Filler content (wt.%)	T_p (°C)	ΔT_p (°C)
INT-WS$_2$	0	92.2	0
	0.1	109.4	17.2
	0.5	117.6	25.4
	1.0	113.6	21.4
[a] MWCNT[14]	0	97.7	0
	0.002	90.3	−7.4
	0.008	96.3	−1.4
	0.02	109.0	11.3
	0.08	109.3	11.6
[b] SWCNT[13]	0	102.8	0
	5	106.5	3.7
	10	105.8	3.0
[b] C60[13]	0	102.8	0
	5	128.8	26.0
	10	116.7	13.9
[c] GO[16]	0	95.1	0
	0.5	97.0	1.9
	1.0	100.4	5.3
	2.0	96.0	0.9
MMT[12]	0	n.p.	—
	1	100.1	—
	3	95.5	—
	5	100.3	—
	7	97.5	—
	9	97.4	—
Nano-CaCO$_3$[11]	0	n.p.	—
	1	n.p.	—
	3	n.p.	—
	5	n.p.	—
Nano-ZnCC[15]	0	n.p.	—
	0.05	118.1	—
	0.1	120.1	—
	0.2	122.0	—
	0.5	123.7	—
	1	125.5	—
	2	126.9	—
	3	128.1	—
N,N′-Bis(benzoyl) suberic acid dihydrazide[10]	0	n.p.	—
	0.5	n.p.	—
	0.8	100	—
	1.0	98	—
	2.0	95	—
	3.0	95	—
Talc[8]	0	n.p.	—
	2	106.9	—
	5	110.9	—
	10	111.1	—
	20	112.6	—
Uraci[19]	0	n.p.	—
	0.1	n.p.	—
	0.2	94.2	—
	0	99.3	—
	1	122.4	—
	2	122.5	—
	5	122.9	—
	10	124.8	—
Phenyl-phosphonic acid[11]	0	n.p.	—
	1	111.2	—
	2	114.9	—
Layered metal phosphonate PPZn[28]	0	n.p.	—
	0.02	120.8	—
	0.05	121.0	—

Table 1 (continued)

Filler	Filler content (wt.%)	T_p (°C)	ΔT_p (°C)
	0.1	122.5	—
	0.5	126.5	—
	1	127.5	—
	2	129.2	—
	5	130.8	—
	10	130.8	—
	15	132.5	—

[a] Cooling rate at 2 °C min^{-1}. [b] Cooling rate at 3 °C min^{-1}. [c] Cooling rate at 5 °C min^{-1}.

(CaCO$_3$),[11] nano-zinc citrate (ZnCC),[15] graphene oxide (GO)[16] and fullerenes (C60)[13] have been shown to provide the added advantage of acting as reinforcements for the polymer. Table 1 summarizes the melt-crystallization data for different PLLA systems incorporating INT-WS$_2$, determined from the exothermic DSC curves obtained at 10 °C min^{-1}, with those attained by the incorporation of nucleating agents and/or nano-sized reinforcements, and Fig. 4 illustrates this comparison by analyzing the difference between the crystallization temperature peak of the composite and that of the neat matrix (ΔT_p) for each. The data clearly show that the addition of INT-WS$_2$ plays a remarkable role in accelerating the crystallization rate of PLLA. The value of $\Delta T_p \sim 25$ °C obtained for an INT-WS$_2$ concentration of 0.5 wt.% far exceeds those attained by the incorporation of other promising nanofillers such as carbon nanotubes and graphene oxide (GO) and is comparable to that observed for a substantially higher concentration of fullerene (C60), *i.e.* 5.0 wt.%. In the same way, layered metal phosphonate (zinc phenylphosphonate, PPZn) has shown excellent nucleating effects on PLLA crystallization (Table 1). With incorporation of 0.02% PPZn, PLLA can finish crystallization under cooling at 10 °C min^{-1}, and the crystallization temperature increases greatly with increasing PPZn concentration (≥ 20 °C).[28]
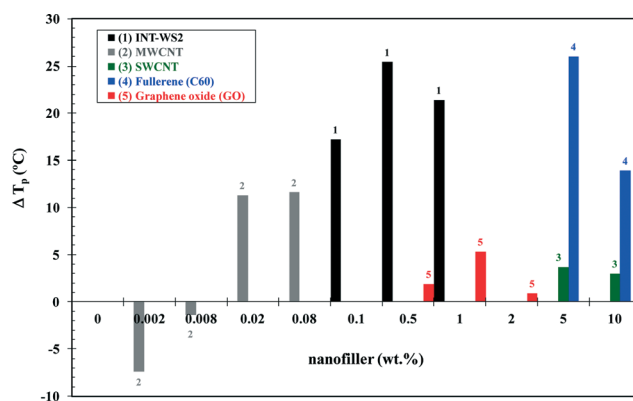

Fig. 4 Increment in the crystallization temperature peak (δt_p) of PLLA systems containing different kinds of nanofillers obtained during cooling at 10 °C min^{-1}.

The degree of crystallinity is also an important index for the characterization of crystallization properties of materials. Fig. 5 displays the dependence of the degree of crystallinity $(1 - \lambda)_c$ of unfilled PLLA resin and filled PLLA nanocomposites on the cooling rate and INT-WS$_2$ loading. The effect of cooling on $(1 - \lambda)_c$ is to be expected because at lower rates macromolecules theoretically have more time for crystallization, which results in fewer defects and thus higher $(1 - \lambda)_c$ (Fig. 5a). This effect is less pronounced in the case of the PLLA/NT-WS$_2$ nanocomposites. That is to say, whereas the crystallinity of PLLA was larger at a slow cooling rate, 56.2% at 1 °C min^{-1}, and became increasingly smaller as the cooling rate was increased, 8.6% at 10 °C min^{-1}, in the case of the 1.0 wt.% of INT-WS$_2$ nanocomposite the change in crystallinity observed was only 5% for the same cooling rates, varying from 59.5 to 54.2%. The influence of INT-WS$_2$ on the crystallinity of PLLA is illustrated in Fig. 5b, where the $(1 - \lambda)_c$ values of PLLA/INT-WS$_2$ are represented at different INT-WS$_2$ loadings. Similar to the results shown in Fig. 3b, the presence of INT-WS$_2$ induces a remarkable increase in the $(1 - \lambda)_c$ value of PLLA in the nanocomposites with respect to neat PLLA at a relatively fast cooling rate of 10 °C min^{-1} ($(1 - \lambda)_c$, PLLA = 8.6%, $(1 - \lambda)_c$, 0.1 wt.% = 50.9%, $(1 - \lambda)_c$, 0.5 wt.% = 53.1%, $(1 - \lambda)_c$, 1.0 wt.% = 54.2%), becoming smaller as the cooling rate was decreased. However, this increment appears to have slight dependence on the concentration of INT-WS$_2$, in agreement with the aforementioned variation of T_p with INT-WS$_2$ contents. It is also important to note that non-isothermal melt-crystallization can be easily observed in the PLLA/INT-WS$_2$ nanocomposites even at a cooling rate of 10 °C min^{-1} (Fig. 2), whereas for neat PLLA at the same rate the crystallization exotherm is hardly observed, indicating that this rate is too fast for neat PLLA to crystallize during non-isothermal melt-crystallization, leading to a low crystallinity value. At cooling rates higher than 10 °C min^{-1}, PLLA basically does not crystallize. However, even with very small amounts of INT-WS$_2$, reasonable levels of crystallinity can be observed, for example in the nanocomposite with 0.1 wt.% INT-WS$_2$ cooled at 20 °C min^{-1}, a value of $(1 - \lambda)_c$ of 28.4% is observed. In brief, the non-isothermal melt-crystallization of PLLA was significantly enhanced in the PLLA/INT-WS$_2$ nanocomposites relative to neat PLLA, which is especially significant at relatively fast cooling rates, indicating that INT-WS$_2$ may act as an effective nucleating agent for PLLA under processing-relevant conditions. Enyashin et al. have deeply studied the role of size and shape of nanoparticles on the nucleation of polymer/IFs using a mesoscopic model of Van der Waals' force field.[29] Specifically, they suggested that in the absence of chemical interaction the size of nanoparticle is a dominating factor for the adhesion strength, while the number of sulfide layers composing the cage is not critical. Certainly, this model may be extended for other morphological types of inorganic (IF/INTs) nanoparticles and utilized in the future for the simulation of different polymer nanocomposites. It is presumed that PLLA crystals might grow on the surface of INT-WS$_2$ by an epitaxial mechanism, as suggested in previous literature for PLLA and other fillers.[7,28] However, additional information is still needed for an in-depth understanding of the exact nucleation mechanism.
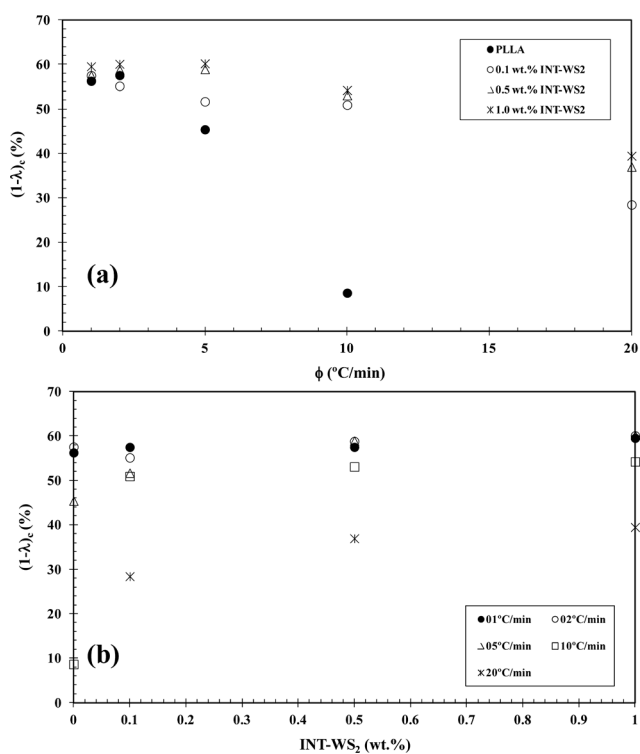
3.4. In situ observation on crystalline structure

To further investigate the formation and growth of PLLA crystals and to determine the crystal modification, synchrotron WAXS was employed to follow the non-isothermal crystallization of the nanocomposites. PLLA can crystallize in α, β, and γ forms.[7] The most common polymorph of PLLA is the α-form, which is believed to grow under the normal conditions such as the melt, cold, or solution crystallization.[7,30,31] The α-form of PLLA with a limiting disordered modification was recently found and defined as the α′-form.[32] The β-form is usually formed upon stretching the polymer at high temperature and high-draw ratio. The γ-form can be obtained via epitaxial crystallization on a hexamethylbenzene (HMB) substrate.[7] In the present case, the samples for the WAXS experiment were prepared by crystallization from the melt, and the samples were expected to crystallize in the α-form. Fig. 6 illustrates the representative WAXS diffractograms obtained during crystallization and subsequent melting for a nanocomposite with 1.0 wt.% INT-WS$_2$. The WAXS profiles always begin with an amorphous halo. With decreasing non-isothermal crystallization temperature, the diffraction peaks appear and gradually intensify, corresponding to formation and growth of the PLLA crystals. The strongest visible diffraction peak in all systems is at 16.7°, which is characteristic of the (200)/(110) reflection of the α-form of PLLA,[7,30,31] whereas no evidence of the characteristic diffraction of α′-crystals[32] at 24.4° was appreciated. This
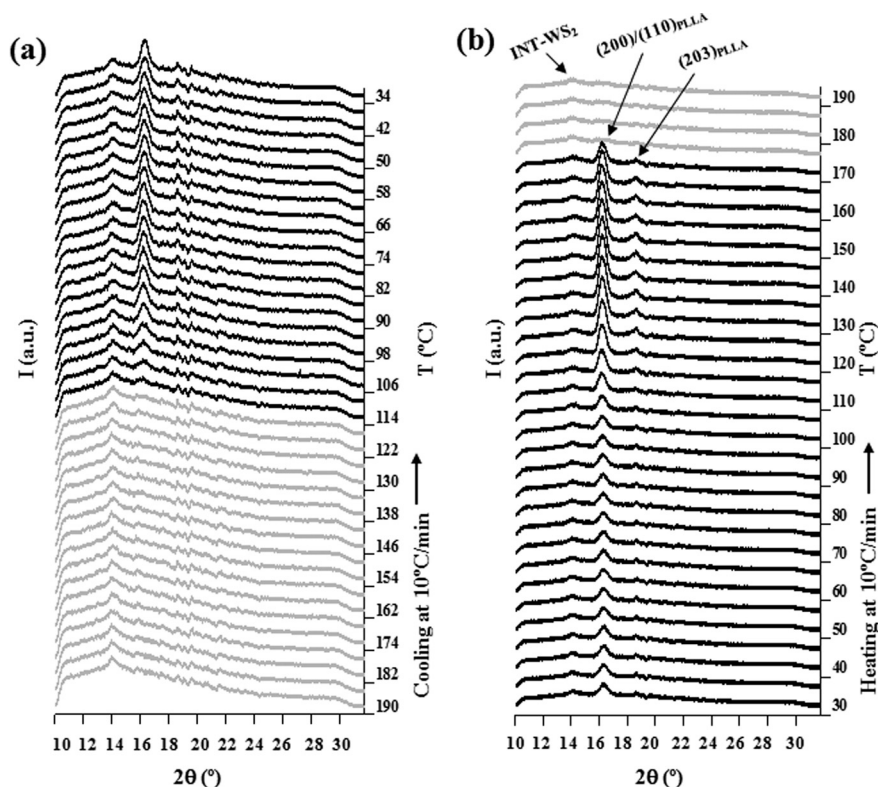

Fig. 5 Variation of the crystallinity $(1 - \lambda)_c$ of PLLA/INT-WS$_2$ with (a) cooling rate and (b) composition.

Fig. 6 WAXS diffractograms of PLLA/INT-WS$_2$ (1.0 wt.%) obtained during (a) cooling from the melt to room temperature at 10 °C min^{-1} and (b) subsequent heating at 10 °C min^{-1}.

implies that the presence of INTs has no impact on the crystalline modification of the PLLA.

3.5. Nucleation activity

Since the crystallization behaviour of PLLA was greatly influenced by INT-WS$_2$ as well as its loading, a quantitative estimation of the nucleation capability of INT-WS$_2$ in a PLLA matrix was undertaken. A common measure of the efficiency of a nucleator is the nucleation activity (φ), whose value varies from 0 to 1, corresponding to extremely active and inert foreign substrates, respectively. In particular, the more active the nucleator is, the lower the value of φ should be. According to Dobreva and Gutzow,[33,34] the nucleation activity can be calculated from the ratio:

$$\varphi = \frac{B^*}{B} \tag{2}$$

where B is a parameter for the pristine polymer and B^* is for the polymer/nucleator system. Both B and B^* can be experimentally determined from the slope of the following equation:

$$\ln \phi = A - \frac{B(\text{or } B^*)}{\Delta T_p^2} \tag{3}$$

where ϕ is the cooling rate, A is a constant, ΔT_p is the supercooling ($T_m - T_p$), T_m is the melting point temperature, and T_p is the crystallization peak temperature. A linear relationship was obtained for each sample, as can be observed in Fig. 7a.

The values of B and B^* are obtained from the slope of the fitted lines, and the nucleation activity (φ) is calculated from this ratio. Thus the values of φ for the PLLA nanocomposites containing 0.1, 0.5 and 1.0 wt.% of INT-WS$_2$ were calculated to be 0.22, 0.23, and 0.25, respectively. It can be observed that the value of φ for INT-WS$_2$ (0.1 wt.%)-nucleated PLLA is much lower than that for pure PLLA ($\varphi = 1$), implying that INT-WS$_2$ actively promotes the nucleation of PLLA. However after a significant fall, the value of φ levels off and is almost independent of the amount of INT-WS$_2$. These results demonstrate that excellent nucleation-promoting effect could be achieved when the concentration of INT-WS$_2$ is selected between 0.1 and 0.5%.

3.6. Effective energy barrier

The crystallization activation energy, or effective energy barrier ΔE, can be used to estimate the growth ability of the chain segments. Considering the variation of the crystallization peak temperature T_p with the cooling rate ϕ, ΔE can be derived from the Kissinger method:[35]

$$\ln\left(\frac{\phi}{T_p^2}\right) = \text{constant} - \frac{\Delta E}{RT_p} \tag{4}$$

where R is the universal gas constant. The activation energies were calculated using the slopes of the lines obtained from plots of $\log \phi/T_p^2$ against $1/T_p$ (Fig. 7b). Thus the values of ΔE for neat PLLA and its nanocomposites containing 0.1, 0.5 and 1.0 wt.% of INT-WS$_2$ were calculated to be −159.2, −96.5,
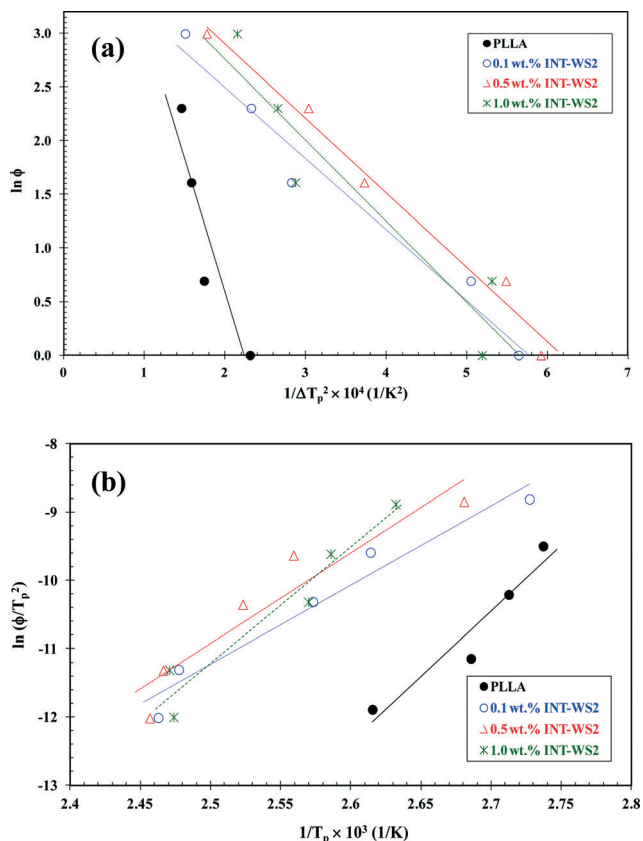
Fig. 7 (a) Dobreva and (b) Kissinger plots for PLLA/INT-WS$_2$ nanocomposites.

and sometimes it is very difficult to differentiate between these two phenomena. However, another possible interpretation in the case of PLLA is due to the phase transition from α′-form crystals to α-crystals and the melting of the as-transformed α crystals.[14,44–46] To date no consensus has been reached as for the exact origin of the multiple melting behaviour of PLLA. Fig. 8 shows the DSC melting thermograms of neat PLLA and PLLA/INT-WS$_2$ nanocomposites recorded at 10 °C min^{-1} subsequent to crystallization from the melt at various cooling rates, and the specific values of the crystalline parameters of all samples are listed in Table 2. During heating, the exothermic peaks attributed to the cold-crystallization process appear for the samples crystallized at higher cooling rates. The appearance of these exothermic peaks indicates that the melt-crystallization process of the samples is incomplete during the prior cooling. As can be seen in Table 2, the cold-crystallization peak temperature ($T_{c,cold}$) of PLLA is influenced by the cooling rate and INT-WS$_2$ loading. In particular, the $T_{c,cold}$ values of PLLA decrease with increasing INT contents (Fig. 9). This suggests that INT-WS$_2$ enhances the cold-crystallization rates of PLLA and thus lowers $T_{c,cold}$. The enhancement of PLLA crystallization, both melt-crystallization and cold-crystallization, by INTs can also be seen from the crystallinity data in Table 2. As an example, as calculated using eqn (1), the $(1 - \lambda)_{c,cold}$ of the samples that were non-isothermally melt-crystallized at 20 °C min^{-1} falls significantly from 41.3% for pure PLLA to 20.3, 9.1 and 5.6 (%) for the PLLA nanocomposites with 0.1, 0.5 and 1.0 wt.% of INT-WS$_2$, respectively.
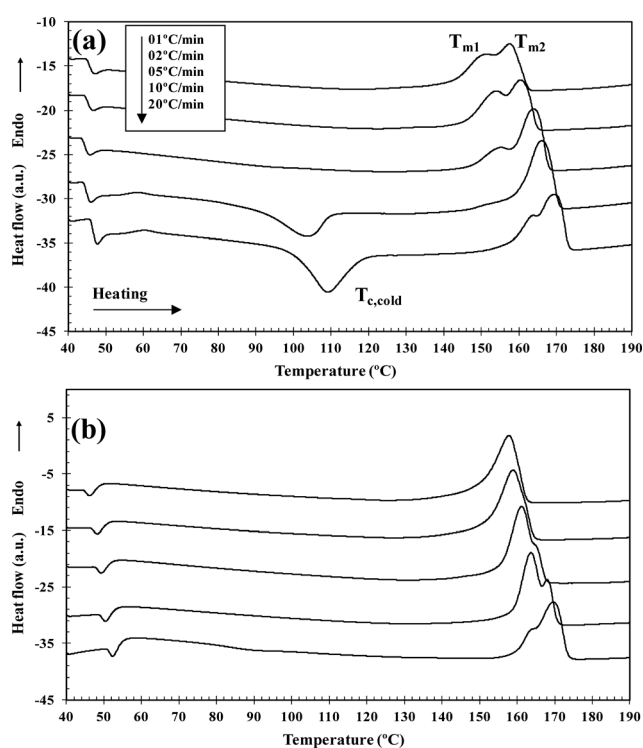
−110.2 and −141.9 kJ mol^{-1}, respectively. ΔE values are negative, indicating that the rate of crystallization increased with decreasing temperature, and the crystallization process of polymer is a barrierless and spontaneous process; the higher the ΔE, the more difficult is the transport of macromolecular segments to the growing surface. As shown, the apparent ΔE values of the nanocomposites vary with the presence of INT-WS$_2$ and rise in the range between −96 and −141 kJ mol^{-1}, indicating that the restriction of molecular mobility of PLLA chains does not appear to be a limiting factor in the crystallization rate, demonstrating that the nucleation activity of INTs plays a dominant role in accelerating the crystallization of PLLA.

3.7. Subsequent melting behaviour of neat PLLA and PLLA/INT nanocomposites crystallized non-isothermally from the melt

The melting of semicrystalline thermoplastics is a very complex process significantly influenced by the crystallization conditions. Multiple melting peaks have been observed in many semicrystalline polymers (e.g. PET, PEEK, etc.) and biodegradable polymers (e.g. PHB, PLLA), which have usually been interpreted in terms of a pre-exiting morphology[36,37] and/or reorganization.[38–43] Both reasons often compete with one another to make the melting behaviour very complex,

Fig. 8 DSC thermograms of melting of (a) PLLA and (b) PLLA/INT-WS$_2$ (0.5 wt.%) obtained after dynamic crystallization at the indicated cooling rates.

Table 2 Crystallization and melting parameters for PLLA/INT-WS$_2$ nanocomposites. s – shoulder

INT-WS$_2$ content (wt.%)	ϕ (°C min^{-1})	T_p (°C)	$(1-\lambda)_c$ (%)	$T_{p,cold}$ (°C)	$(1-\lambda)_{c,cold}$ (%)	T_{m1} (°C)	T_{m2} (°C)	$(1-\lambda)_m$ (%)	φ^a	ΔE^b (kJ mol^{-1})
0.0	1	109.2	56.2	—	—	151.6	157.7	54.6	1.00	−159.2
	2	99.2	57.5	—	—	154.3	160.5	53.4		
	5	95.5	45.4	92.0	3.3	155.6	163.9	51.5		
	10	92.2	8.6	104.2	30.0	152.7 s	166.1	51.0		
	20	—	—	109.4	41.3	164.3 s	170.1	48.0		
0.1	1	132.9	57.7	—	—	—	169.8	52.4	0.22	−96.5
	2	130.5	55.1	—	—	—	169.8	50.2		
	5	115.5	51.7	—	—	165.6	170.3	51.0		
	10	109.4	50.9	—	—	164.5	170.6	57.5		
	20	93.5	28.4	97.9	20.3	—	169.3	51.0		
0.5	1	132.5	57.3	—	—	—	158.2	60.0	0.23	−110.2
	2	132.3	58.6	—	—	—	159.2	61.5		
	5	123.2	58.7	—	—	161.4 s	164.9	60.8		
	10	117.6	52.8	—	—	163.9	168.3	56.4		
	20	99.9	36.8	90.2	9.1	164.3 s	169.7	50.3		
1.0	1	131.1	59.5	—	—	—	162.4	61.0	0.25	−141.9
	2	131.6	60.1	—	—	—	167.2	64.1		
	5	116.0	60.2	—	—	154.3	160.5	56.0		
	10	113.6	54.2	95.3	—	155.3	161.1	54.5		
	20	106.8	39.4	97.1	5.6	155.8	161.9	54.2		

[a] Nucleation activity calculated using Dovreba's equation. [b] Effective energy barrier calculated using Kissinger's equation.

Fig. 8a also compares the evolution of the double endothermic peaks for pure PLLA and PLLA/INT-WS$_2$ as a function of the cooling rate. The endothermic curve broadened with increasing cooling rates. According to these results, the melting behaviour has been associated with one or two melting peaks depending on the cooling rates (the peak at the lower temperature is denominated T_{m1} and that at the higher temperature, T_{m2}). As the cooling rate was increased, the T_{m2} peak area increased while the T_{m1} peak area decreased, indicating that the T_{m2} peak arises from the rearrangement of the initial crystal morphology (*i.e.* melting–recrystallization–melting) and that the T_{m1} peak represents the melting of original crystals formed when the sample was cooled from the melt. In particular, the magnitude of the area of T_{m2} becomes larger with respect to that of T_{m1} with increasing cooling rate, indicating that the melting–recrystallization–melting of PLLA is enhanced with increasing cooling rate. The aforementioned results are reasonable because the time for PLLA to crystallize becomes shorter with increasing

cooling rate. Thus, the crystals formed during the dynamic crystallization are not as perfect or stable, and they will recrystallize and reorganize into more perfect and stable crystals during the subsequent heating scan. Therefore, T_{m2} grows and becomes dominant when the high cooling rates are used. It is also necessary to note the disappearance of the melting–recrystallization–melting behaviour of PLLA (at a low cooling rate), indicating that the presence of INT-WS$_2$ enhances the crystallization rate of PLLA in the nanocomposites. Therefore, the crystals in the nanocomposites are more perfect and stable than those in neat PLLA especially when the low cooling rate is used, and T_{m1} is more dominant in the nanocomposites than in neat PLLA.

3.8. Dynamic mechanical properties

In order to obtain information on the effect of INT-WS$_2$ on the mechanical properties of PLLA, dynamic mechanical properties were measured. Fig. 10 shows the temperature-dependent storage modulus (E') and loss factor (tan δ) for pure PLLA and PLLA/INT-WS$_2$ (1.0 wt.%). It is clear that the storage modulus of PLLA nanocomposites is higher than that of pure PLLA at low temperature in the glassy state, indicating stiffness enhancement through the addition of INT-WS$_2$. For example, the value of E' = 3127 MPa for pure PLLA at room temperature increases to 3630, 3640 and 3590, respectively, upon increasing the INT-WS$_2$ contents from 0.1 to 1.0 wt.%. Furthermore, one can observe a slight increment in E' at temperatures between 90 and 130 °C, which can be attributed to the cold crystallization process occurring during the heating process. Fig. 10 also compares the loss factor (tan δ) for different samples. It is generally accepted that a higher amplitude of tan δ is associated with higher chain mobility, and the area of the tan δ peak is usually related to the content of amorphous phase. Furthermore, the tan δ peak position also represents the
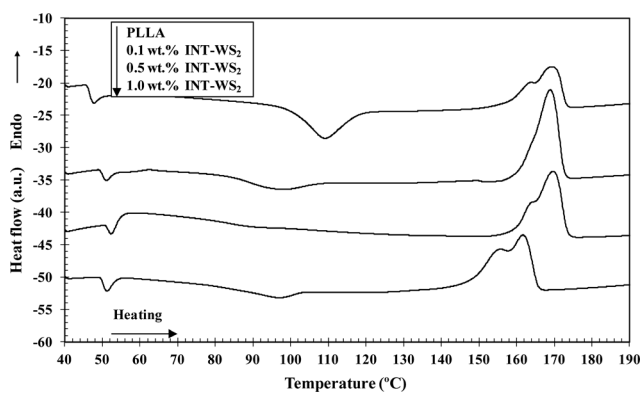

Fig. 9 DSC thermograms of melting of neat PLLA and its nanocomposites obtained after non-isothermal crystallization at 20 °C min^{-1}.
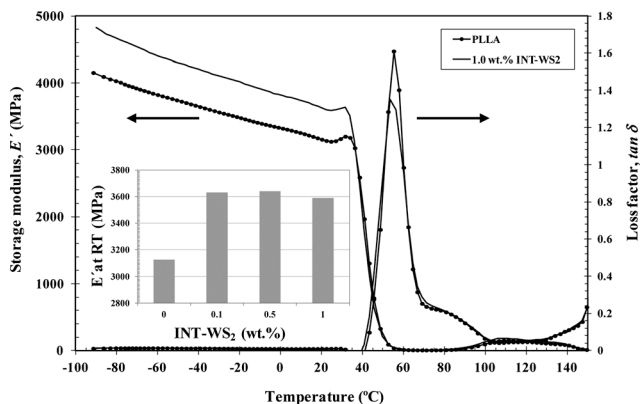
Fig. 10 Dynamic mechanical spectra of PLLA/INT-WS$_2$ nanocomposites obtained in the tensile mode at 1 Hz; the inset shows the room temperature values of storage modulus (E') of PLLA *versus* INT-WS$_2$ concentration.

T_g of chain segments in the amorphous region. In this study, the presence of INT-WS$_2$ leads to a decrease in the intensity of tan δ, indicating that the nanofiller imposes some restrictions on the mobility of the PLLA chain segments. No detectable variation in peak positions of PLLA/INTs is observed with the change of composition.

Conclusions

In the present investigation, inorganic nanotubes (INT-WS$_2$) were well-dispersed into a PLLA matrix through simple melt-blending, and the thermomechanical properties were studied. The results obtained from the DSC analysis show that the cooling rate and INT-WS$_2$ contents are very efficient factors for the control of the overall crystallization rate and crystallinity of PLLA. In particular, it was shown that INT-WS$_2$ exhibits higher nucleation efficiency, improving the melt- and cold-crystallization behaviour of PLLA. The presence of INTs has no impact on the crystalline modification of the PLLA. The addition of only 0.1 wt.% of INT-WS$_2$ allowed crystallization of PLLA at a cooling rate of 10 °C min^{-1}, and the crystallization peak temperature (T_p) increases significantly, by up to 17 °C, corresponding to the highest value observed hitherto for PLLA formulations using nano-sized fillers (*e.g.* MWCNT, SCWCNT, C60, and GO). Moreover, the melting of PLLA is found to be also greatly influenced by INT-WS$_2$ loadings and cooling rates. The two melting peaks of PLLA can be attributed to the melting–recrystallization–melting mechanism. In particular, it was found that increasing the INT-WS$_2$ loadings and decreasing the cooling rates restricted the occurrence of the recrystallization of PLLA in the nanocomposites. The disappearance of this phenomenon indicated that the presence of INT-WS$_2$ enhances the crystallization rate PLLA in the nanocomposites, and more perfect and stable crystals are observed than those in neat PLLA especially when the low cooling rate is used. More significantly, the addition of INT-WS$_2$ is an effective method to enhance the cold-crystallization rate of PLLA by reducing both the crystallization temperature

($T_{p,cold}$) and the crystallinity $(1 - \lambda)_{c,cold}$. These features may be advantageous for the enhancement of the mechanical properties (storage modulus) and processability of PLLA-based materials. In this respect, these observations will enable the development of advanced PLLA formulations for many applications and open the way to the production of PLLA parts with greater thermal and mechanical performance. This is a clear example of an alternative strategy that overcomes the limitations of polymer nanocomposites, *i.e.* performance, cost effectiveness and processability, offering new prospects in the preparation of advanced biopolymer materials. The results obtained from thermal and dynamic-mechanical experiments encourage further investigations in order to evaluate the full potential of these new nanocomposites for use in many eco-friendly and medical applications.

References

1 R. E. Drumright, P. R. Gruber and D. E. Henton, *Adv. Mater.*, 2000, **12**, 1841–1846.
2 R. G. Sinclair, *Pure Appl. Chem.*, 1996, **33**, 585–597.
3 H. Tian, Z. Tang, X. Zhuang, X. Chen and Z. Jing, *Prog. Polym. Sci.*, 2012, **37**, 237–280.
4 A. Sodergard and M. Stolt, *Prog. Polym. Sci.*, 2002, **27**, 1123–1163.
5 L. T. Lim, R. Auras and M. Rubino, *Prog. Polym. Sci.*, 2008, **33**, 820–882.
6 R. M. Rasal, A. V. Janrkor and D. E. Hirt, *Prog. Polym. Sci.*, 2010, **35**, 338–356.
7 S. Saeidou, M. A. Huneault, H. Li and C. B. Park, *Prog. Polym. Sci.*, 2012, **37**, 1657–1677.
8 A. M. Harris and E. C. Lee, *J. Appl. Polym. Sci.*, 2008, **107**, 2246–2255.
9 P. Pan, J. Yang, G. Shan, Y. Bao, Z. Weng and Y. Inoue, *Macromol. Mater. Eng.*, 2012, **297**, 670–679.
10 Y. Cai, S. Yan, J. Yin, Y. Fan and X. Chen, *J. Appl. Polym. Sci.*, 2011, **121**, 1408–1416.
11 L. Han, C. Han, J. Bian, Y. Bian, H. Lin, X. Wang, H. Zhang and L. Dong, *Polym. Eng. Sci.*, 2012, **52**, 1474–1484.
12 F. Ublekov, J. Baldrian, J. Kratochvil, M. Steinhart and E. Nedkov, *J. Appl. Polym. Sci.*, 2012, **124**, 1643–1648.
13 H. Tsuji, Y. Kawashima, H. Takikawa and S. Tanaka, *Polymer*, 2007, **48**, 4213–4225.

14 H. S. Xu, X. J. Dai, P. R. Lamb and Z. M. Li, *J. Appl. Polym. Sci.*, 2009, **47**, 2341–2352.

15 P. Song, G. Chen, Z. Wei, Y. Chang, W. Zhang and J. Liang, *Polymer*, 2012, **53**, 4300–4309.

16 H. Wang and Z. Qiu, *Thermochim. Acta*, 2012, **527**, 40–46.

17 R. Tenne, L. Margulis, M. Genut and G. Hodes, *Nature*, 1992, **360**, 444–445.

18 L. Margulis, G. Salitra, R. Tenne and M. Talianker, *Nature*, 1993, **365**, 113–114.

19 A. Zak, L. Sallacan-Ecker, A. Margolin, M. Genut and R. Tenne, *NANO*, 2009, **4**, 91–98.

20 A. Zak, L. Sallacan Ecker, N. Fleischer and R. Tenne, *Sens. Transducers J.*, 2011, **12**, 1–10.

21 M. Naffakh, A. M. Díez-Pascual, C. Marco, G. Ellis and M. A. Gómez-Fatou, *Prog. Polym. Sci.*, 2013, **38**, 1163–1231.

22 E. Zohar, S. Baruch, M. Shneider, H. Dodiu, S. Kenig, D. H. Wagner, A. Zak, A. Moshkovith, L. Rapoport and R. Tenne, *Sens. Transducers J.*, 2011, **12**, 53–65.

23 C. S. Reddy, A. Zak and E. Zussman, *J. Mater. Chem.*, 2011, **21**, 16086–16093.

24 G. Lalwani, A. M. Henslee, B. Farshid, P. Parmar, L. Lin, Y. X. Qin, F. K. Mikos, A. G. Kasper and B. Sitharaman, *Acta Biomater.*, 2013, **9**, 8365–8373.

25 E. W. Fischer, H. J. Sterzel and G. Wegner, *Kolloid Z. Z. Polym.*, 1973, **251**, 980–990.

26 E. Lizundia, S. Petisco and J. R. Sarasua, *J. Mech. Behav. Biomed. Mater.*, 2013, **17**, 242–251.

27 B. Kalb and A. Pennings, *J. Polym. Sci., Polym. Chem. Ed.*, 1980, **21**, 607–612.

28 P. Pan, Z. Liang, A. Cao and Y. Inoue, *ACS Appl. Mater. Interfaces*, 2009, **1**, 402–411.

29 A. N. Enyashin and P. Y. Glazyrina, *Phys. Chem. Chem. Phys.*, 2012, **14**, 7104–7111.

30 J. Kobayashi, T. Asahi, M. Ichiki, A. Oikawa, H. Suzuki, T. Watanabe, E. Fukada and Y. Shikinami, *J. Appl. Phys.*, 1995, **77**, 2957–2973.

31 C. Alemán, B. Lotz and J. Puiggalí, *Macromolecules*, 2001, **34**, 4795–4801.

32 J. M. Zhang, Y. X. Duan, H. Sato, H. Tsuji, I. Noda, S. K. Yan and Y. Ozaki, *Macromolecules*, 2005, **38**, 8012–8021.

33 A. Dobreva and I. Gutzow, *J. Non-Cryst. Solids*, 1993, **162**, 1–12.

34 A. Dobreva and I. Gutzow, *J. Non-Cryst. Solids*, 1993, **162**, 13–25.

35 H. E. Kissinger, *J. Res. Natl. Bur. Stand.*, 1956, **57**, 217–221.

36 P. Cebe and S. D. Hong, *Polymer*, 1986, **27**, 1183–1192.

37 D. C. Bassett, R. H. Olley and I. A. M. Raheil, *Polymer*, 1988, **29**, 1745–1754.

38 P. J. Holdsworth and A. T. Jones, *Polymer*, 1971, **12**, 195–208.

39 Y. Lee and R. S. Porter, *Macromolecules*, 1987, **20**, 1336–1341.

40 Y. Lee, R. S. Porter and J. S. Lin, *Macromolecules*, 1989, **22**, 1756–1760.

41 A. M. Jonas, T. P. Russell and D. Y. Yoon, *Macromolecules*, 1995, **28**, 8491–8503.

42 J. Quian, L. Zhu, J. Zhang and R. S. Whitehouse, *J. Polym. Sci., Part B: Polym. Phys.*, 2007, **45**, 1564–1577.

43 M. Yasuniwa, S. Tsubakihara, Y. Sugimoto and C. Nakafuku, *J. Polym. Sci., Part B: Polym. Phys.*, 2004, **42**, 25–32.

44 P. J. Pan, W. H. Kai, B. Zhu, T. Dong and Y. Inoue, *Macromolecules*, 2007, **40**, 6898–6905.

45 P. J. Pan, W. H. Kai, B. Zhu, T. Dong and Y. Inoue, *Macromolecules*, 2008, **41**, 4296–4304.

46 P. Song, G. Chen, Z. Wei, W. Zhang and J. Liang, *J. Therm. Anal. Calorim.*, 2013, **111**, 1507–1514.